# Engineering Design of Outer-Selective Tribore Hollow Fiber Membranes for Forward Osmosis and Oil-Water Separation

**Xue Li, Wan Lin Ang, Yingda Liu, and Tai-Shung Chung**
Dept. of Chemical & Biomolecular Engineering, National University of Singapore, Singapore 117585, Singapore

*DOI 10.1002/aic.15012*
*Published online August 25, 2015 in Wiley Online Library (wileyonlinelibrary.com)*

*Outer-selective thin-film composite (TFC) hollow fiber membranes offer advantages like less fiber blockage in the feed stream and high packing density for industrial applications. However, outer-selective TFC hollow fiber membranes are rarely commercially available due to the lack of effective ways to remove residual reactants from fiber's outer surface during interfacial polymerization and form a defect-free polyamide film. A new simplified method to fabricate outer-selective TFC membranes on tribore hollow fiber substrates is reported. Mechanically robust tribore hollow fiber substrates containing three circular-sector channels were first prepared by spinning a P84/ethylene glycol mixed dope solution with delayed demixing at the fiber lumen. The thin wall tribore hollow fibers have a large pure water permeability up to 300 L* $m^{-2}$ $h^{-1}$ $bar^{-1}$*. Outer-selective TFC tribore hollow fiber membranes were then fabricated by interfacial polymerization with the aid of vacuum sucking to ensure the TFC layer well-attached to the substrate. Under forward osmosis studies, the TFC tribore hollow fiber membrane exhibits a good water flux and a small flux difference between active-to-draw (i.e., the active layer facing the draw solution) and active-to-feed (i.e., the active layer facing the feed solution) modes due to the small internal concentration polarization. A hyperbranched polyglycerol was further grafted on top of the newly developed TFC tribore hollow fiber membranes for oily wastewater treatment. The membrane displays low fouling propensity and can fully recover its water flux after a simple 20-min water wash at 0.5 bar from its lumen side, which makes the membrane preferentially suitable for oil-water separation.* © 2015 American Institute of Chemical Engineers *AIChE J*, 61: 4491–4501, 2015

*Keywords: tribore hollow fibers, forward osmosis process, thin-film composite membrane, outer-selective, oil-water separation*

## Introduction

With limited freshwater resources and stringent regulations in wastewater discharge, extensive research has been focused on membrane development for wastewater reuse. Currently, integrally skinned asymmetric membranes are prevailing in microfiltration and ultrafiltration applications, while thin-film composite (TFC) membranes are dominant in osmotic processes such as reverse osmosis (RO), forward osmosis (FO), and pressure retarded osmosis (PRO).[1–12] The TFC membranes consist of an ultrathin polyamide selective layer to reduce the transport resistance and a porous substrate to provide the mechanical strength. Typically, the polyamide selective layer is formed by the interfacial polymerization between *m*-phenylenediamene (MPD) in an aqueous phase and 1,3,5-trimesoyl chloride (TMC) in an organic phase, as shown in Scheme 1.[9] Interfacial polymerization also provides advantages of choosing various monomers and substrates that give tunability in membrane morphology and performance.[7,8,13–17] However, one drawback of TFC membranes is the sophistication of fabrication. As a result, most commercially available TFC membranes are in the flat-sheet configuration. A few inner-selective TFC hollow fiber membranes have been demonstrated,[14,17,18] but outer-selective ones are rare in the literature.[19]

Outer-selective TFC hollow fiber membranes provide various advantageous for commercial applications. First, they are less inclined to fiber blockage and have a less pressure drop along the fiber module than the inner-selective ones due to lower mass-transfer resistance in the shell side.[19,20] Second, the dimension of outer-selective hollow fiber membranes can be much smaller than inner-selective ones. Thus, the former not only can increase the packing density in a module, but also offer a much higher active area than the latter if they have the same fiber diameter. These features make the former more efficient and desirable for commercial purposes.[19] However, it is much more difficult to fabricate outer-selective hollow fiber membranes than their inner-selective counterparts, especially for large-scale commercial production.[9,19] The primary obstacle is the fabrication of a perfect polyamide film without defects. Ineffective removal of the residual amine solution from the outer fiber surface not only produces unfavorable pin-hole as defects, but also makes neighboring fibers stick together. As a consequence, the fibers stick together and the resultant polyamide layer grows in the space among fibers

Additional Supporting Information may be found in the online version of this article.

Correspondence concerning this article should be addressed to T. S. Chung at chencts@nus.edu.sg.

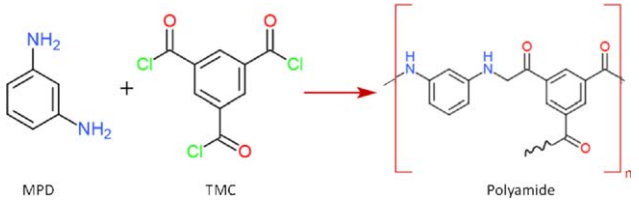


**Scheme 1. Interfacial polymerization reaction between MPD and TMC.**

**[Color figure can be viewed in the online issue, which is available at wileyonlinelibrary.com.]**

instead of on each fiber surface, leading to a defective polyamide dense layer. To overcome it, Sun and Chung[19] had developed a method of vacuum-assisted dip-coating interfacial polymerization to remove the excess amine solution from outer surfaces and fabricated outer-selective TFC hollow fiber membranes. However, their method was delicate and time consuming because of multiple steps. Therefore, the first objective of this study was to examine the feasibility of fabricating outer-selective TFC hollow fiber membranes with desirable morphologies and robust mechanical properties by a shortened and simplified method using P84 (Supporting Information Figure S1) as the substrate.

The second objective of this study is to fabricate outer-selective TFC tribore hollow fiber membranes for FO applications. Thin wall single-bore hollow fiber membranes often have poor mechanical properties as an unavoidable consequence of being highly porous and highly permeable. Hence, single-bore hollow fiber membranes would break easily during prolonged operations. Multibore membranes such as rectangular multibore membranes[21–23] and multibore hollow fibers[24–28] have gained considerable interests over the past years. Not only have they shown superior mechanical properties but also separation performance in comparison to the single-bore hollow fibers. So far, only one inner selective tribore paper has been published for FO,[28] no outer selective tribore FO membranes have been studied. Therefore, this work may provide useful implications toward the fabrication of outer-selective TFC tribore membranes for FO applications.

FO has been demonstrated successfully for the treatment of oil-water emulsions,[29–32] but its serious fouling issue has to be settled urgently. Therefore, the third objective of this study is to investigate if we can graft the newly developed outer-selective TFC tribore hollow fiber membrane by hyperbranched polyglycerol (HPG) to enhance its antifouling properties for oily wastewater treatment.

## Experimental

### *Materials and chemicals*

P84 copolyimide (BTDA-TDI/MDI, copolyimide of 3,3′,4,4′-benzophenone tetra-carboxylic dianhydride and 80% methylphenylene diamine +20% methylene diamine) was purchased from HP Polymer, Austria. Supporting Information Figure S1 shows its chemical structure. The solvent *N*-methyl-2-pyrrolidinone (NMP, >99.5%) and nonsolvent ethylene glycol (EG, 99.9%) were ordered from Merck and VWR, respectively, and were used to prepare the spinning solutions. The deionized water used in experiments was produced by a Milli-Q ultrapure water system (Millipore). A 50/50 wt % mixture of glycerol (Industrial grade, Aik Moh Paints & Chemicals Pte., Singapore) and deionized water was prepared to post-treat as-spun hollow fiber supports before drying. Polyethylene glycol 2000, 4000, 6000, and 10,000 (PEG, $M_w = 2000$ g mol$^{-1}$, 4000 g mol$^{-1}$, 6000 g mol$^{-1}$, and 10,000 g mol$^{-1}$, respectively, Merck) were employed to characterize the molecular weight cutoff (MWCO), mean pore size and pore-size distribution of hollow fiber supports. Triethylamine (TEA, 99%), *m*-phenylenediamine (MPD, >99%), 1,3,5-benzenetricarbonyl trichloride (TMC, 98%), dopamine hydrochloride (99%), tris(hydroxymethyl)aminomethane (Tris, ≥99.8%), sodium dodecyl sulfate (SDS, >99%), and polyethylene glycol 400 (PEG 400, $M_w = 400$ g mol$^{-1}$, 99.0%) were bought from Sigma-Aldrich. Hexane (reagent grade) and sodium chloride (NaCl) were procured from Merck. Oil-water emulsions (10,000 ppm) were prepared by use of Happy Family branded soya bean oil procured from a local supermarket and Tween 80 surfactant. All chemicals were used as received.

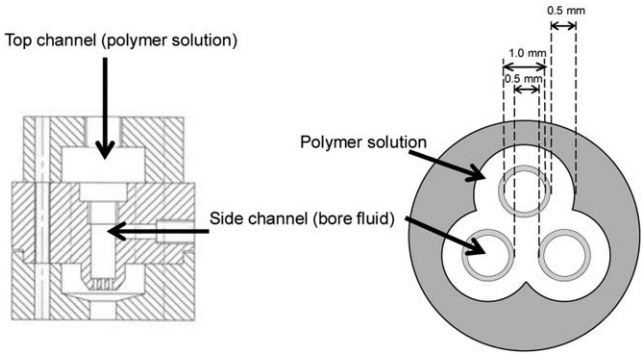


**Figure 1. Schematic design of the tribore blossom spinneret.**

### *Fabrication of tribore hollow fiber supports and post-treatment*

Prior to preparing polymer solutions, the P84 polymer powder was dried overnight at 90 ± 5°C in a vacuum oven. The dehydrated P84 polymer was dissolved in a NMP/EG solution with a composition of 21/10/69 wt % P84/EG/NMP, where NMP is a solvent, EG is a weak nonsolvent.[33–35] After the spinning, dope solution was prepared, it was degassed for several hours and then stored in a 500-mL syringe pump (ISCO) overnight before spinning. The P84 hollow fiber supports were spun by a dry-jet wet spinning process as described in the literature.[17,36–38] Table 1 summarizes spinning conditions such as polymer solution flow rate, bore fluid flow rate, and air gap to investigate their effects on fiber morphologies, dimensions, and performance. A tribore blossom spinneret illustrated in Figure 1 was employed in this work. After spinning, the as-spun hollow fiber supports were rinsed with tap water for 2 days to remove residual solvents and EG. A glycerol/water mixture (50/50 wt %) was used to soak hollow fiber supports for another 2 days, and then they were dried in air at room temperature. Soaking membranes in the glycerol/water mixture might minimize the pore collapse during drying.[39–42] Hollow fiber modules were fabricated using Swagelok stainless fittings. A slow curing epoxy resin (EP 231, Kuo Sen, Taiwan) was used for module potting. The length of the potting portion for each end was around 3 cm.

### *Fabrication of outer-selective TFC membranes*

The TFC polyamide membrane was synthesized on the outer surface of P84 hollow fiber supports by interfacial

Table 1. Spinning Conditions of P84 Tribore Hollow Fiber Membranes

| Spinning Parameter | Hollow Fiber Code | | |
|---|---|---|---|
| | I | II | III |
| Polymer solution (wt %) | | P84/EG/NMP: 21/10/69 | |
| Polymer solution flow rate (mL $min^{-1}$) | 3 | 4 | 8 |
| Bore fluid composition (wt %) | | DI water/NMP (5/95) | |
| Bore fluid flow rate (mL $min^{-1}$) | 2 | 3 | 5.5 |
| Air gap (cm) | 5 | 1 | 1 |
| External coagulant | | Tap water (room temperature) | |
| Take up speed (m $min^{-1}$) | | 9.35 | |
| Spinneret | | Tribore blossom | |

polymerization: (1) a PEG 400 (0.5 wt %) aqueous solution was pumped and circulated through the shell-side of the membrane module at a flow rate of 28 mL $min^{-1}$ for 30 min; (2) a MPD/TEA/SDS (2/0.0625/0.1wt %) aqueous solution was then pumped into the shell side of the module at a flow rate of 28 mL $min^{-1}$ and surrounded the fibers for 5 min, while simultaneously applying vacuum from the lumen side at 800 mbar for the same duration; (3) after the MPD solution was drained from the module, vacuum was further applied from the lumen side of hollow fibers for a particular duration; (4) a 0.15 wt % TMC solution in hexane was pumped into the shell side at a flow rate of 28 mL $min^{-1}$ for 5 min; (5) the TMC solution was drained out and the module was dried in ambient air for 1 h with a humidity from 60 to 80%; (6) the resultant TFC membrane was washed thoroughly with deionized water and stored in deionized water before subsequent tests.

The antifouling layer consisted of a polydopamine (PDA) coating and a HPG polymer grafting. PDA acts as a linkage between the support and the HPG grafting layer by strong noncovalent interactions with the support and covalent bondings with thiol groups of HPG. First, 0.4 g of 3-hydroxytyramine hydrochloride (dopamine HCl) was polymerized under ambient air and aqueous conditions in a 200 mL solution of 0.02 M Tris buffer at pH 8.5. This solution was pumped and circulated in the shell side of the module for 3 h. Second, a mixture of 10 g $L^{-1}$ deoxygenated thiolated HPG (prepared as described in the previous publication[38]) and 0.175 vol % TEA was pumped into the shell side of the module so that the outer surfaces of the TFC hollow fiber membranes were soaked in the mixture for 16 h. The grafted TFC membrane was then washed thoroughly by deionized water and stored in deionized water before subsequent tests.

### *Characterizations*

The membrane morphology was examined by a field emission scanning electron microscope (FESEM, JEOL JSM-6700F). Before tests, samples were fractured in liquid nitrogen followed by platinum coating using a Jeol JFC-1100E Ion Sputtering device. Membrane surface topology was studied using a Nanoscope IIIa atomic force microscope (AFM) from Digital Instruments. Each membrane sample was scanned at a rate of 1.00 Hz using the tapping mode.

Porosity measurements were conducted as per the protocol reported elsewhere.[8] Fresh wet membranes were removed from the water bath and dabbed dry with tissue papers. Care was taken to ensure that all visible water droplets were well removed and that excess water confined in the lumen side of the hollow fiber membranes was removed. The membranes were then weighed to obtain the weight of wet membranes, $m_1$ (g), freeze dried overnight, and reweighed to obtain the weight of dry membranes, $m_2$ (g). The water content confined within the pores was then determined via $(m_1 - m_2)$. The overall porosity ($\varepsilon$) can be calculated as

$$\varepsilon(\%) = \frac{(m_1 - m_2)/\rho_{\text{water}}}{(m_1 - m_2)/\rho_{\text{water}} + m_2/\rho_{\text{polymer}}} \times 100\% \quad (1)$$

The characteristics of P84 porous substrates such as pore size, MWCO, and pore-size distribution were measured by the solute transport method as described elsewhere.[17,43,44] PEG solutions with a concentration of 200 ppm, each comprising a different molecular weight, were used to measure the solute rejection under a hydraulic pressure difference of 1 bar. The concentrations of the neutral solutes were measured by a total organic carbon analyzer (TOC ASI-5000A, Shimadzu, Japan).

The measured feed ($C_f$) and permeate ($C_p$) concentrations were used for the calculation of the effective solute rejection coefficient $R_s$ (%)

$$R_s = \left(1 - \frac{C_p}{C_f}\right) \times 100\% \quad (2)$$

According to the Einstein equation, a Stokes radius which describes the solute dimension could be expressed as

$$D_{AB} = \frac{kT}{6r\pi\eta} \quad (3)$$

where $r$ is the Stokes radius, $D_{AB}$ is the diffusivity, $k$ is the Boltzmann constant, and $\eta$ is the solvent viscosity. Conversely, the diffusivity is also a function of the intrinsic viscosity $[\eta]$[45]

$$D_{AB} = \frac{2.5 \times 10^6 kT}{\eta (M_w[\eta])^{1/3}} \quad (4)$$

where $M_w$ is the molecular weight. Combining Eqs. 2 and 3 yields the following equation for the Stokes radius of the solute as a function of $M_w$ and $[\eta]$[46–48]

$$r = 2.12 \times 10^{-8} \times (M_w[\eta])^{1/3} \quad (5)$$

As a result, the solute diameters $d_s$ (nm) of PEG (Eq. 5) can be determined as follows

$$d_s = 3.35 \times 10^{-2} \times M_w^{0.557} \quad (6)$$

The mean effective pore size and the pore-size distribution were then obtained according to the traditional solute transport approach by ignoring the influence of the steric and hydrodynamic interaction between solute and membrane pores, the mean effective pore size ($\mu_p$) and the geometric standard deviation ($\sigma_p$) can be assumed to be the same as $\mu_s$ (the geometric mean size of solute at $R_s = 50\%$) and $\sigma_g$ (the geometric

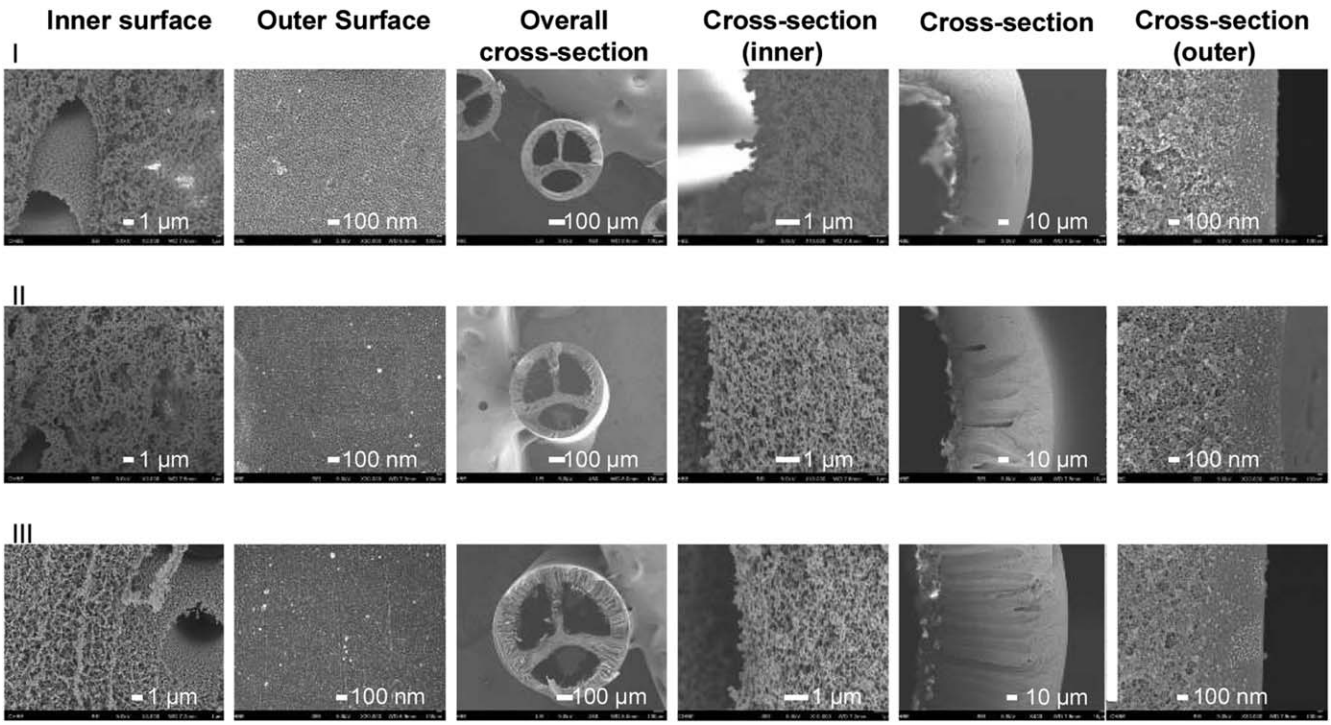


**Figure 2. SEM morphologies of as-spun P84 tribore hollow fiber membranes as functions of spinning conditions.**

standard deviation defined as the ratio of the $d_s$ at $R_s = 84.13\%$ over that at $R_s = 50\%$). The MWCO was determined at $R_s = 90\%$. Therefore, based on $\mu_p$ and $\sigma_p$, the pore-size distribution of a membrane can be expressed as the following probability density function[44]

$$\frac{dR(d)^p}{dd_p} = \frac{1}{d_p \ln \sigma_p \sqrt{2\pi}} \exp\left[-\frac{(\ln d_p - \ln \mu_p)^2}{2(\ln \sigma_p)^2}\right] \quad (7)$$

The pure water permeability (PWP) of the membrane supports was determined by testing the membranes using a lab-scale circulating filtration unit that has been described elsewhere.[28,43,49] Pure water feed was applied into the shell-side of a hollow fiber module containing three hollow fiber supports at a constant pressure of 1 bar at room temperature. Permeates from the PWP experiments were then collected and measured to determine the PWP.

Mechanical properties of membranes including the elongation at break, maximum tensile strength, and Young's modulus were measured at the constant elongation rate of 10 mm $min^{-1}$ with a starting gauge length of 50 mm by an Instron tensiometer (Model 5542, Instron Corp.). Six samples were tested to minimize the experimental error and ensure the accuracy. The collapse pressure was calculated by the Barlow's equation based on tensile stress and fiber dimension[18]

$$P = \frac{2\chi T}{\mathrm{OD} \times \mathrm{SF}} \quad (8)$$

where $\chi$ is the wall thickness, $T$ is the maximum tensile stress, OD is the outer diameter, and SF is the safety factor (usually SF = 1).

### *Membranes performance in FO tests*

The FO tests were conducted on a lab-scale FO setup using membrane modules as described in previous publications.[28,50] Model RO retentate (1 M NaCl) and deionized water were used as draw and feed solutions, respectively. TFC membranes were oriented in the active-to-draw mode (i.e., the active layer facing the draw solution or so called the PRO mode) or in active-to-feed mode (i.e., the active layer facing the feed

**Table 2. Mechanical Properties, Dimension, and Porosity in P84 Hollow Fiber Membranes**

| | Hollow Fiber Code | | |
|---|---|---|---|
| | I | II | III |
| Elongation at break (%) | 34.3 ± 3.8 | 21.7 ± 3.4 | 30.8 ± 8.1 |
| Tensile strength (MPa) | 4.8 ± 0.4 | 3.6 ± 0.2 | 4.7 ± 0.3 |
| Young's modulus (MPa) | 230.4 ± 22.0 | 123.5 ± 6.9 | 138.4 ± 14.4 |
| Toughness[a] ($\times 10^6$ J $m^{-3}$) | 1.41 ± 0.21 | 0.62 ± 0.15 | 1.38 ± 0.20 |
| OD ($\mu$m) | 778.2 ± 26.8 | 1133.0 ± 34.5 | 1319.2 ± 34.0 |
| Wall thickness ($\mu$m) | 100.1 ± 10.5 | 156.0 ± 10.5 | 180.1 ± 14.0 |
| Porosity (%) | 74.4 ± 1.0 | 72.1 ± 1.0 | 73.5 ± 0.4 |
| PWP (LMH/bar) at 1 bar | 299.2 ± 58.4 | 175.2 ± 41.8 | 173.1 ± 52.7 |
| Collapse pressure[b] (bar) | 12.3 | 9.9 | 12.8 |

[a]Calculated by taking the integral underneath the stress-strain curve.
[b]Calculated by the Barlow's equation.

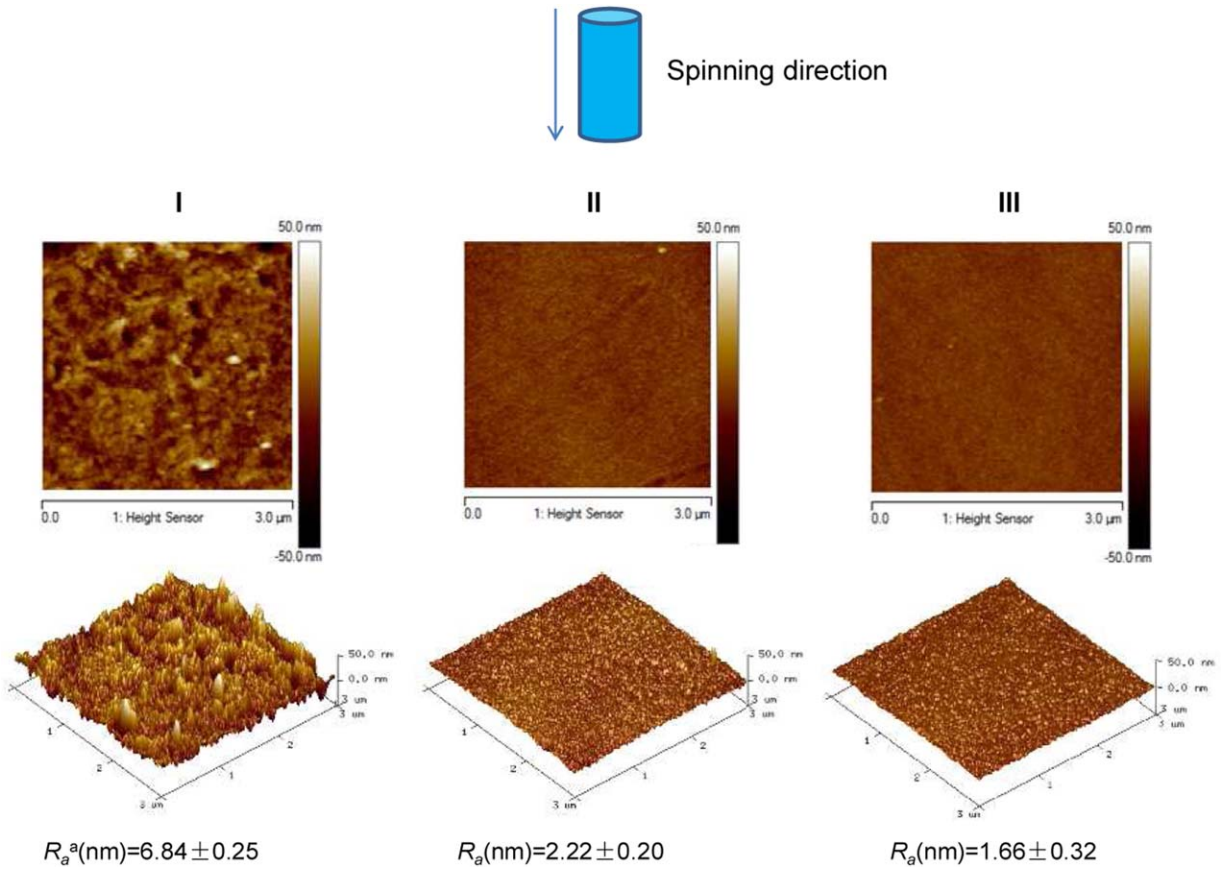


**Figure 3. AFM images of outer surfaces of as-spun hollow fiber membranes ($R_a$ is the mean roughness).**

**[Color figure can be viewed in the online issue, which is available at wileyonlinelibrary.com.]**

solution or the FO mode). A variable-speed gear pump (Masterflex, Easy-Load II Model 77200-50) was employed for solution recirculation. In all experiments, there was no hydraulic pressure applied on the membrane and pressure build-up as a result of fluid flow.

For oil-water separation, experiments were carried out in the active-to-feed mode (i.e., FO mode). An oil-water emulsion feed of 10,000 ppm was prepared according to the previous publication.[29] This oil-water emulsion was then utilized as the feed solution when a model RO retentate was used as the draw solution. An initial water flux was obtained under the same conditions in the absence of foulants. After tests, back washing was performed with a pressure of 0.5 bar for 20 min.

## Results and Discussion

### *Morphology and surface roughness of hollow fiber supports*

Figure 2 displays morphologies of P84 hollow fiber supports (from I to III) spun from different spinning conditions via the tribore spinneret. The hollow fibers have a center-symmetric round shape outer geometry and three circular-sector inner bores. The round outer geometry is resulted from several combined factors such as (1) the balance of surface energy to lower the overall energy, (2) die swell, (3) rapid phase inversion at the outer surface due to the employment of a strong external coagulant (i.e., water), and (4) delay demxing (i.e., a slow phase inversion) at the lumen because of using a weak bore fluid of water/NMP (5/95 wt %). The slow phase inversion at the lumen not only helps the nascent fiber to redistribute the stresses during the phase inversion but also rearranges its inner structure under the elongational stretch. Consequently, a circular-sector shape is formed to minimize the overall energy and stresses. Moreover, the addition of NMP into the bore fluid and EG into the dope solution leads to a slower precipitation rate, and then enhances the delayed demixing.[51–53] Hence, all hollow fiber supports exhibit a highly porous structure on inner surfaces with relatively dense outer surfaces. The fully porous inner layer makes the three

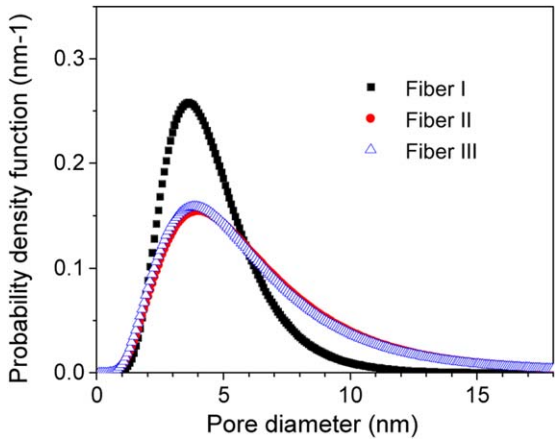


**Figure 4. Probability density function curves of tribore hollow fiber membranes.**

**[Color figure can be viewed in the online issue, which is available at wileyonlinelibrary.com.]**

**Table 3. Pore-Size Characteristics of Tribore Hollow Fiber Membranes**

| Pore Characteristics | Hollow Fiber Code | | |
|---|---|---|---|
| | I | II | III |
| Mean pore diameter (nm) | 4.22 ± 0.29 | 5.43 ± 0.15 | 5.27 ± 0.04 |
| Geometric standard deviation | 1.49 ± 0.03 | 1.74 ± 0.06 | 1.75 ± 0.02 |
| MWCO (kDa) | 13.57 ± 2.65 | 29.88 ± 0.78 | 28.42 ± 0.07 |

circular-sector bore channels highly interconnected with robust mechanical properties.

According to the cross-sectional images, fiber I has few macrovoids, while fibers II and III possess many macrovoids. As fiber I was spun from the smallest dope and bore fluid rates with the highest air gap, the elongational stress and air gap may help retard the formation of macrovoids.[52–55] In contrast, higher dope and bore flow rates with a short air gap were utilized to spin fibers II and III; the high dope rate tends to result in a thick wall with macrovoids,[52,55,56] while the high bore fluid rate may induce local surface instabilities on the nascent fibers,[53,57] eventually giving rise to the undesirable macrovoids. Table 2 tabulates the mechanical properties, dimension, and porosity of these hollow fiber membranes. Fiber I has the smallest dimension and wall thickness with the highest PWP of 299.2 L $m^{-2}$ $h^{-1}$ $bar^{-1}$ at 1 bar.

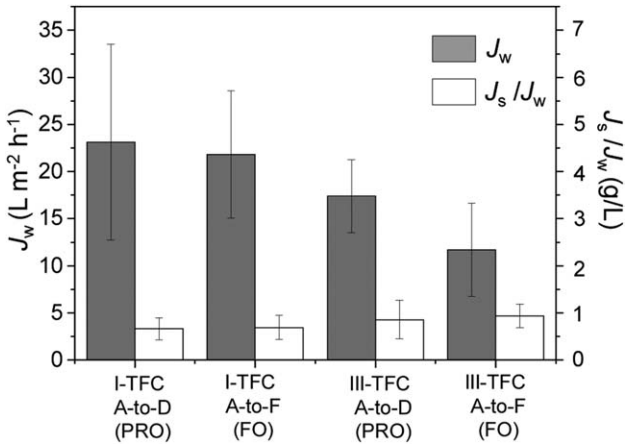


**Figure 7. Water flux and salt to water flux ratio of TFC hollow fiber membranes.**

**The draw solution is 1 M NaCl. The feed solution is deionized water. A-to-D: Active-to-draw (i.e., PRO mode); A-to-F: Active-to-feed (i.e., FO mode).**

Figure 3 shows the AFM images and surface roughnesses of the outer surfaces of hollow fiber supports. All fiber supports have relatively smooth surface topologies with small roughnesses around 1–7 nm. Among them, hollow fiber I is slightly rougher than the other two, probably due to its small bore-

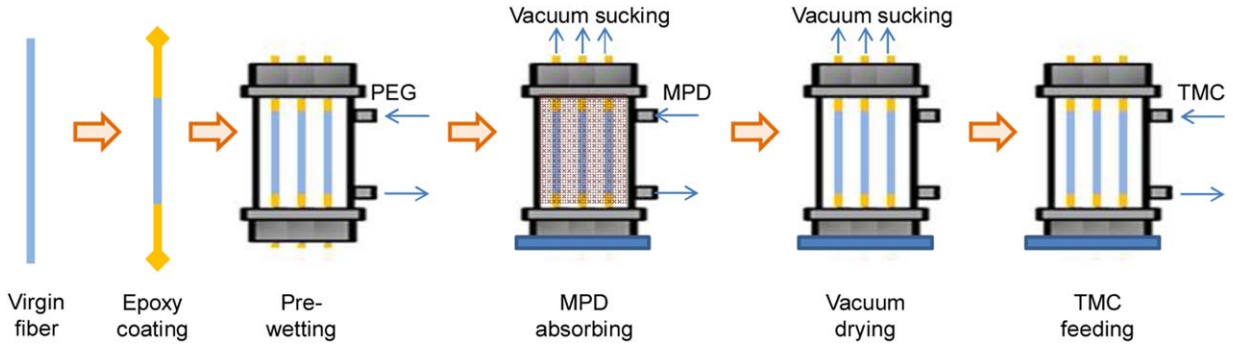


**Figure 5. Schematic procedure for the fabrication of outer-selective TFC hollow fiber membranes.**

**[Color figure can be viewed in the online issue, which is available at wileyonlinelibrary.com.]**

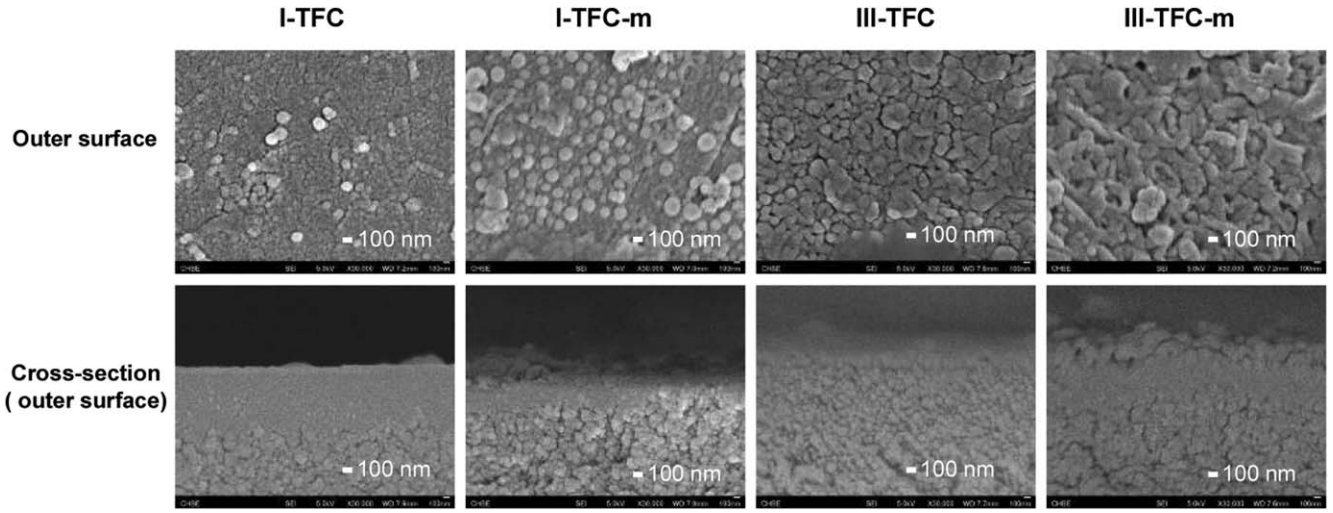


**Figure 6. SEM morphologies of active polyamide layers (TFC layers) of TFC hollow fiber membranes.**

**HPG modified TFC membranes are designated as "TFC-m."**

**Table 4. Transport Properties of TFC Membranes**

| Membrane | Water Permeability, $A$ (L m$^{-2}$ h$^{-1}$ bar$^{-1}$) | Salt Permeability, $B$ (L m$^{-1}$ h$^{-1}$) | $S_t$ ($\times$ 10$^{-4}$ m) |
|---|---|---|---|
| I-TFC | 1.22 ± 0.36 | 0.048 ± 0.024 | 2.32 ± 0.74 |
| III-TFC | 0.71 ± 0.31 | 0.021 ± 0.001 | 4.72 ± 1.17 |
| I-TFC-m | 0.95 ± 0.10 | 0.023 ± 0.012 | 3.69 ± 0.48 |
| III-TFC-m | 0.66 ± 0.13 | 0.021 ± 0.007 | 6.78 ± 1.02 |

NaCl (1000 ppm) as the feed solution in RO tests under an applied pressure of 1 bar.

fluid flow rate. In other words, the high bore-fluid flow rates may expand the outer surfaces of fibers II and III during the rapid phase inversion and result in smooth and similar nanostructures, while the outer surface of fiber I may shrink and create roughness because of rapid solvent exchange (i.e., solvents leach out) and a small bore-fluid flow rate.

### *Pore characteristics and mechanical properties of hollow fiber supports*

Table 3 summarizes the pore characteristics of the hollow fiber supports, while Figure 4 illustrates their probability density function curves. Fiber I has the smallest mean pore size of 4.22 nm and lowest MWCO of 13.57 kDa, while fibers II and III have comparable pore sizes and MWCO values. The air-gap induced orientation is mainly responsible for the smaller pores.[52,53,58] In other words, the nascent fiber is stretched and oriented by gravity in the axial direction as the macromolecules have yet to undergo a complete solidification process in the air gap region. Consequently, pores and polymer chains with higher air gaps would tend to be stretched and aligned in comparison to similar nascent fibers with lower air gaps. Similar phenomena have been observed.[50–52]

The mechanical properties listed in Table 2 confirm our hypotheses. Because of the air-gap induced orientation, fiber I has good mechanical properties in terms of elongation at break, tensile strength, Young's modulus, and toughness. The highest Young's modulus of fiber I indicates its highest stiffness among these hollow fibers. Even though fiber I has a much thinner wall compared with fiber III (100 vs. 180 $\mu$m), the former has a comparable collapse pressure with the latter (12.3 vs. 12.8 bar). As fibers I and III have good mechanical properties, they are adopted for the subsequent TFC membrane fabrications.

### *Fabrication of outer-selective TFC hollow fiber membranes and their FO performance*

Figure 5 illustrates the procedure to fabricate the module and conduct interfacial polymerization. Both ends of each fiber are first sealed by epoxy to prevent the fiber lumen and potting region from any reactant. To ensure that fibers do not contact one another during and after interfacial polymerization, the fibers are well-distributed and well-spaced out to leave a space between each other or from the module wall. Thereafter, the fibers are pretreated with a 0.5 wt % PEG400 aqueous solution for 30 min to improve their wettability. Then, a MPD solution is pumped into the shell side of module to saturate the fibers for 5 min. Different from the previous approach by Sun and Chung,[19] vacuum is applied for the entire duration of the MPD adsorbing in the present study.

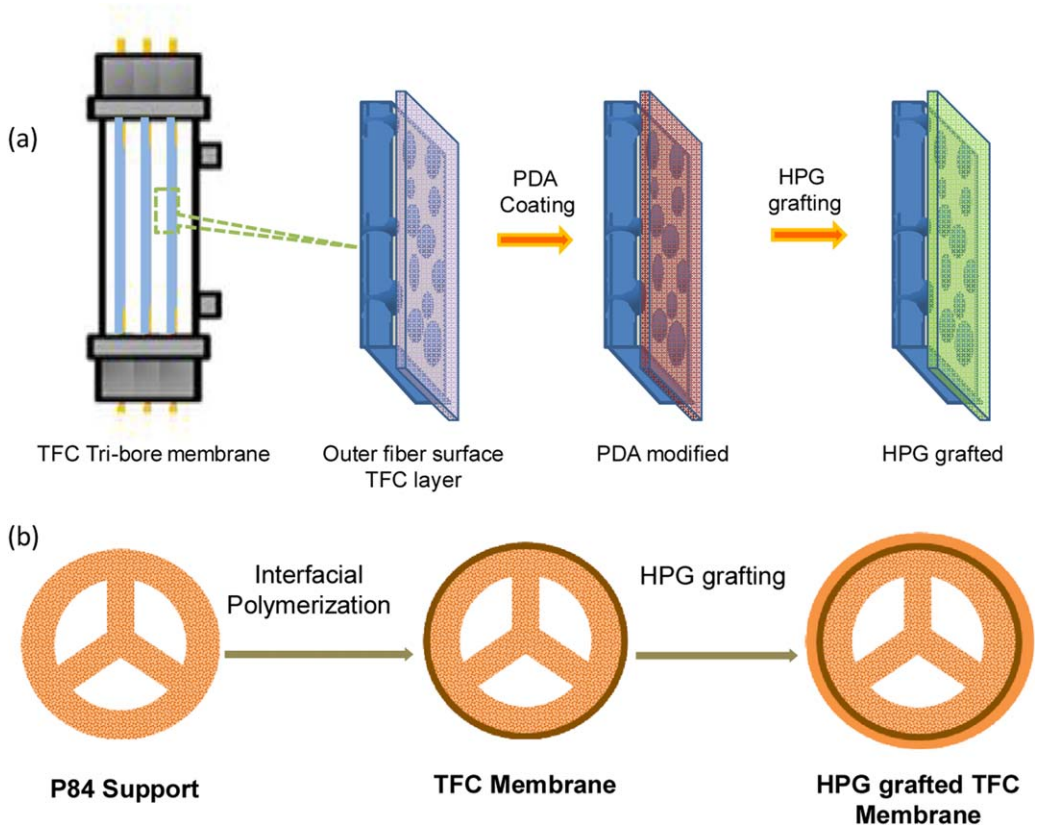


**Figure 8. Schematic procedure for the antifouling modification on TFC hollow fiber membranes [(a) side view; (b) top view on each fiber].**

**[Color figure can be viewed in the online issue, which is available at wileyonlinelibrary.com.]**

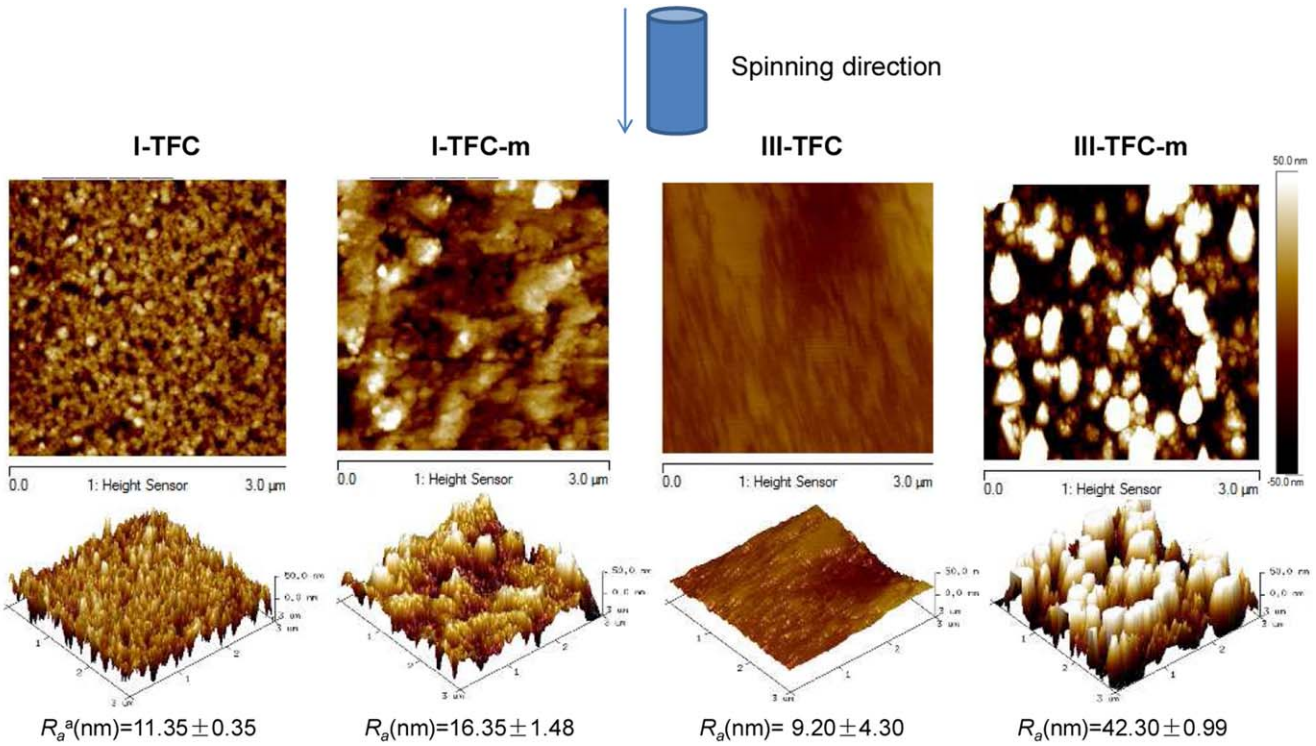


**Figure 9. AFM images of active polyamide layers (TFC layers) of P84-TFC hollow fiber membranes ($R_a$ is the mean roughness).**

**[Color figure can be viewed in the online issue, which is available at wileyonlinelibrary.com.]**

Supporting Information Figure S2 illustrates different situations of MPD soaking in the previous interfacial polymerization; fibers might or might not have been fully saturated with MPD. To avoid it, vacuum is conducted simultaneously with the MPD adsorbing in this study to ensure that hollow fiber supports are fully saturated with MPD.

After MPD absorbing, vacuum sucking is also conducted to remove the excess MPD. A critical vacuum condition where the exact amount of excess MPD solution is removed, would subsequently lead to a well-attached polyamide dense layer on the substrate. Otherwise, an undercritical vacuum condition where the excess MPD solution is left on the substrate surface, would result in a loosely attached polyamide layer; or an overcritical vacuum condition where the MPD solution retreats into the substrate pores, would leave defects on the resultant polyamide layer. Supporting Information Figure S3 illustrates the membrane performance of III-TFC with different vacuum durations. Clearly, a critical vacuum time of 10 min gives the

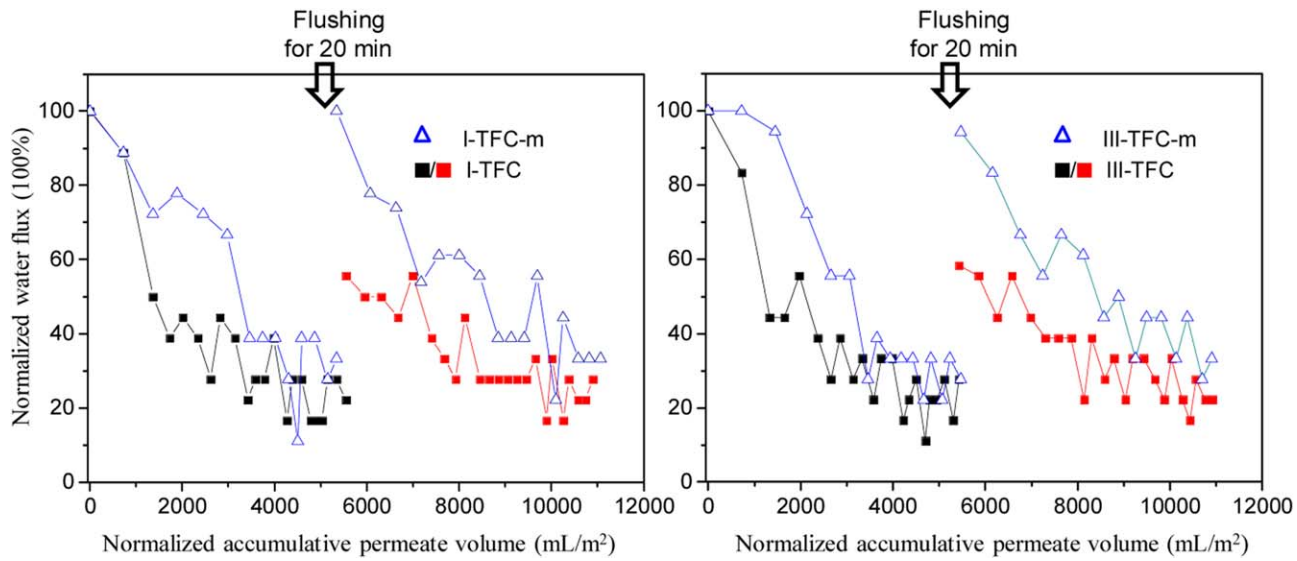


**Figure 10. Membrane fouling performance using a 10,000 ppm oil-water emulsion as the feed.**

**The normalized water flux decline is plotted against the normalized accumulative permeate flux. The draw solution initially contained 1 M NaCl. Tests were conducted in the active-to-feed mode. [Color figure can be viewed in the online issue, which is available at wileyonlinelibrary.com.]**

highest water flux with lowest salt leakage. After the removal of excess MPD solution, the TMC solution is pumped into the module shell to react with the MPD molecules on top of the hollow fibers, followed by a drying in air to stabilize the nascent TFC layer. In the new interfacial polymerization process, it not only shortens the time, but also eliminates the need of post-treatment of glycerol soaking for pore opening, making the new method simpler.

Figure 6 shows the active polyamide layers (i.e., TFC layers) of TFC hollow fiber membranes after interfacial polymerization on their outer surfaces. The TFC layer of the I-TFC membrane consists of many small globules and few worm-like domains, while the III-TFC membrane is fully covered with large ridges. The increase in feature size of the TFC layer agrees well with our previous study[50] where large substrate pores are capable of facilitating large polyamide ridges.

FO experiments were conducted on the I- and III-TFC membranes using a cross-flow system. Figure 7 compares the FO performance. In the active-to-draw mode (i.e., PRO mode), the III-TFC tribore hollow fiber membrane has a water flux ($J_w$) of 17.4 L $m^{-2}$ $h^{-1}$ and a $J_s/J_w$ ratio (i.e., the ratio of reverse salt flux to water flux) of 0.9 g $L^{-1}$ when using 1 M NaCl and deionized water as the feed pair. In contrast, this membrane has a water flux of 11.7 L $m^{-2}$ $h^{-1}$ and a $J_s/J_w$ ratio of 0.9 g $L^{-1}$ in the active-to-feed mode (i.e., FO mode). The difference can be ascribed to the fact that the active-to-draw mode has less internal concentration polarization (ICP) than the active-to-feed mode.[59] In the case of the I-TFC membrane, it has a water flux of 23.1 L $m^{-2}$ $h^{-1}$ in the active-to-draw mode and a flux of 21.8 L $m^{-2}$ $h^{-1}$ in the active-to-feed mode. Their $J_s/J_w$ ratios are about 0.7 g $L^{-1}$, respectively. These values are lower than other outer-selective TFC membranes[19] because the I-TFC tribore membrane has less ICP effect due to its high porosity and thin wall. Table 4 lists their transport properties. I-TFC membrane has a very low salt permeability coefficient $B$, a comparable water permeability coefficient $A$. Importantly, I-TFC has an excellent structural parameter $S_t$ of $2.32 \pm 0.74 \times 10^{-4}$ m, indicating much less ICP inside the porous layer. The advantage of being less suffered from ICP makes the I-TFC tribore hollow fiber membrane preferential in the osmotic process for oil-water separation.

### *Investigation of performance for outer-selective TFC hollow fiber membranes in oily wastewater treatment*

To expand the newly developed tribore membrane for oily wastewater treatment and to lower the fouling propensity led by oil, a HPG grafting layer was introduced to the outer surface of the TFC hollow fibers, as illustrated in Figure 8. Figure 6 displays the SEM images of HPG-grafted TFC membranes, while Figure 9 shows the corresponding AFM images. The HPG-grafted TFC membranes have much rougher surfaces than their pristine TFC counterparts. Clearly, the HPG polymers attached to polyamide ridges dramatically amplify the ridge structure and thus enhance the surface roughness. Conversely, the grafting of PDA and HPG layer slightly amplifies resistances to water and salt. In FO tests (active-to-feed mode), the I-TFC-m membrane has a smaller water flux ($J_w$) of 15.3 L $m^{-2}$ $h^{-1}$ and a $J_s/J_w$ ratio of 0.8 g $L^{-1}$ when using 1 M NaCl and deionized water as the feed pair. Similarly, the III-TFC-m membrane shows a $J_w$ of 9.6 L $m^{-2}$ $h^{-1}$ and a $J_s/J_w$ ratio of 0.9 g $L^{-1}$ at the same conditions. The transport permeabilities of modified membranes also decrease to some extent, as a result of the PDA coating and HPG grafting.

Figure 10 shows the FO performance of four TFC membranes in a high concentration oil-water emulsion. The normalized water flux is plotted against the normalized accumulative permeate volume. The solid symbols indicate the normalized water flux of the pristine TFC membranes, while empty dots represent the water flux of HPG-grafted TFC membranes. For pristine TFC membranes, immediately after the testing, the water flux substantially declines to less than 50%; then, gradually drops to about 20% of the initial flux when the normalized permeate volume is 5500 mL $m^{-2}$. The HPG-grafted TFC membranes undergo smoother flux declines, and reach a plateau about 35–40% of the initial water flux. After tests and before the next test, a back washing by deionized water was performed at 0.5 bar from the lumen side of the hollow fiber membranes for 20 min. The back washing obtains an easy recovery of water flux to original levels (>94%) in cases of HPG-grafted membranes, but only allows a partial recovery of 56–58% for pristine TFC membranes. It can be summarized that modified outer-selective TFC tribore hollow fiber membranes are effective in water treatments.

## Conclusions

We have strategically designed novel and efficient methods for the fabrication of outer-selective tribore hollow fiber membranes via interfacial polymerization and HPG grafting for FO and oil-water separation. First, novel tribore hollow fiber supports with a high degree of concentricity and minimal defects were designed. Second, a simplified method was developed to synthesize a thin-film dense polyamide layer on top of these hollow fiber supports. Third, a HPG grafting was deposited on top of the TFC layer with enhanced antifouling properties for oily wastewater treatment. The following conclusions can be drawn from this work:

1. Spinning conditions play important roles to determine the mechanical properties, pore size, and pore-size distribution of the as-spun tribore hollow fiber supports. A large air gap and a moderate bore fluid help produce tribore hollow fiber supports with better mechanical properties, narrower pore-size distribution, and higher flux.
2. A good attachment between the polyamide dense layer and the hollow fiber support was demonstrated if vacuum was always applied during MPD absorbing and the removal of excess MPD solution.
3. Using 1 M NaCl and deionized water as the feed pair, the newly developed I-TFC membrane displays a water flux of 23.1 L $m^{-2}$ $h^{-1}$ in the active-to-draw mode (i.e., PRO mode) and a flux of 21.8 L $m^{-2}$ $h^{-1}$ in the active-to-feed mode (i.e., FO mode) with a low $J_s/J_w$ ratio of about 0.7 g $L^{-1}$ due to its high porosity, thin wall, and small ICP effect.
4. The HPG-grafted TFC tribore hollow fibers are effective in the treatment of oil-water emulsions with robust mechanical stabilities and low fouling propensity. The I-TFC-m membrane can fully recover its water flux after a simple 20-min cleaning at 0.5 bar from its lumen side.

## Acknowledgments

This research was supported by the National Research Foundation, Prime Minister's Office, Singapore "Advanced FO Membranes and Membrane Systems for Wastewater Treatment, Water Reuse and Seawater Desalination" (Grant numbers: R-279-000-336-281 and R-278-000-339-281).

Special thanks are due to Mr. Zhenlei Cheng, Ms Dan Hua, Mr. Damon Petersen, Mr. Paul Antonio, and Dr. Peng Wang for their useful comments and assistance.

## Literature Cited


1. Nunes SP, Peinemann K-V. *Membrane Technology in the Chemical Industry*. Germany: Wiley-VCH Verlag GmbH, 2001.
2. Zeman LJ, Zydney AL. *Microfiltration and Ultrafiltration: Principles and Applications*. New York: Marcel Dekker, Inc., 1996.
3. Lemanski J, Lipscomb G. Effect of shell-side flows on hollow-fiber membrane device performance. *AIChE J*. 1995;41:2322–2326.
4. Escobar IC, Bruggen BVD. *Modern Applications in Membrane Science and Technology*. Washington, DC: American Chemical Society, 2011.
5. Taniguchi M, Kimura S. Estimation of transport parameters of RO membranes for seawater desalination. *AIChE J*. 2000;46:1967–1973.
6. Petersen RJ. Composite reverse-osmosis and nanofiltration membranes. *J Membr Sci*. 1993;83:81–150.
7. Bui NN, McCutcheon JR. Hydrophilic nanofibers as new supports for thin film composite membranes for engineered osmosis. *Environ Sci Technol*. 2013;47:1761–1769.
8. Li X, Chung TS. Effects of free volume in TFC membranes on osmotic power generation. *AIChE J*. 2013;59:4749–4761.
9. Lau WJ, Ismail AF, Misdan N, Kassim MA. A recent progress in thin film composite membrane: a review. *Desalination*. 2012;287: 190–199.
10. Xu J, Feng X, Gao C. Surface modification of thin-film-composite polyamide membranes for improved reverse osmosis performance. *J Membr Sci*. 2011;370:116–123.
11. Saeki D, Tanimoto T, Matsuyama H. Anti-biofouling of polyamide reverse osmosis membranes using phosphorylcholine polymer grafted by surface-initiated atom transfer radical polymerization. *Desalination*. 2014;350:21–27.
12. Shishatskiy S, Nistor C, Popa M, Nunes SP, Peinemann K-V. Comparison of asymmetric and thin-film composite membranes having Matrimid 5218 selective layer. *Desalination*. 2006;199:193–194.
13. McCutcheon JR, Elimelech M. Modeling water flux in forward osmosis: implications for improved membrane design. *AIChE J*. 2007;53:1736–1744.
14. Wang R, Shi L, Tang CY, Chou S, Qiu C, Fane AG. Characterization of novel forward osmosis hollow fiber membranes. *J Membr Sci*. 2010;355:158–167.
15. Chung TS, Li X, Ong RC, Ge QC, Wang HL, Han G. Emerging forward osmosis (FO) technologies and challenges ahead for clean water and clean energy applications. *Curr Opin Chem Eng*. 2012;1: 246–257.
16. Fam W, Phuntsho S, Lee JH, Cho J, Shon HK. Boron transport through polyamide-based thin film composite forward osmosis membranes. *Desalination*. 2014;340:11–17.
17. Li X, Chung TS. Thin-film composite P84 co-polyimide hollow fiber membranes for osmotic power generation. *Appl Energy*. 2014;114: 600–610.
18. Zhang S, Sukitpaneenit P, Chung TS. Design of robust hollow fiber membranes with high power density for osmotic energy production. *Chem Eng J*. 2014;241:457–465.
19. Sun SP, Chung TS. Outer-selective pressure-retarded osmosis hollow fiber membranes from vacuum-assisted interfacial polymerization for osmotic power generation. *Environ Sci Technol*. 2013;47:13167–13174.
20. Sivertsen E, Holt T, Thelin W, Brekke G. Pressure retarded osmosis efficiency for different hollow fibre membrane module flow configurations. *Desalination*. 2013;312:107–123.
21. Peng N, Teoh MM, Chung TS, Koo LL. Novel rectangular membranes with multiple hollow holes for ultrafiltration. *J Membr Sci*. 2011;372:20–28.
22. Bonyadi S, Mackley M. The development of novel micro-capillary film membranes. *J Membr Sci*. 2012;389:137–147.
23. Spruck M, Hoefer G, Fili G, Gleinser D, Ruech A, Schmidt-Baldassari M, Rupprich M. Preparation and characterization of composite multichannel capillary membranes on the way to nanofiltration. *Desalination*. 2013;314:28–33.
24. Gille D, Czolkoss W. Ultrafiltration with multi-bore membranes as seawater pre-treatment. *Desalination*. 2005;182:301–307.
25. Bu-Rashid KA, Czolkoss W. Pilot tests of multibore UF membrane at Addur SWRO desalination plant, Bahrain. *Desalination*. 2007; 203:229–242.
26. Wang P, Luo L, Chung TS. Tri-bore ultra-filtration hollow fiber membranes with a novel triangle-shape outer geometry. *J Membr Sci*. 2014;452:212–218.
27. Hua D, Ong YK, Wang P, Chung TS. Thin-film composite tri-bore hollow fiber (TFC TbHF) membranes for isopropanol dehydration by pervaporation. *J Membr Sci*. 2014;471:155–167.
28. Luo L, Wang P, Zhang S, Han G, Chung TS. Novel thin-film composite tri-bore hollow fiber membrane fabrication for forward osmosis. *J Membr Sci*. 2014;461:28–38.
29. Duong PHH, Chung TS. Application of thin film composite membranes with forward osmosis technology for the separation of emulsified oil–water. *J Membr Sci*. 2014;452:117–126.
30. Li P, Lim SS, Neo JG, Ong RJ, Weber M, Staudt C, Widjojo N, Maletzko C, Chung TS. Short and long term performance of the thin-film composite forward osmosis (TFC-FO) hollow fiber membranes for oily wastewater purification. *Ind Eng Chem Res*. 2014;53: 14056–14064.
31. Zhang S, Wang P, Fu XZ, Chung TS. Sustainable water recovery from oily wastewater via forward osmosis-membrane distillation (FO-MD). *Water Res*. 2014;52:112–121.
32. Coday BD, Xu P, Beaudry EG, Herron J, Lampi K, Hancock NT, Cath TY. The sweet spot of forward osmosis: treatment of produced water, drilling wastewater, and other complex and difficult liquid streams. *Desalination*. 2014;333:23–35.
33. Kim JH, Lee KH. Effect of PEG additive on membrane formation by phase inversion. *J Membr Sci*. 1998;138:153–163.
34. Krok M, Pamula E. Poly(L-lactide-co-glycolide) microporous membranes for medical applications produced with the use of polyethylene glycol as a pore former. *J Appl Polym Sci*. 2012;125:E187–E199.
35. Ali M, Zafar M, Jamil T, Butt MTZ. Influence of glycol additives on the structure and performance of cellulose acetate/zinc oxide blend membranes. *Desalination*. 2011;270:98–104.
36. Ishigami T, Kasuya Y, Rajabzadeh S, Ohmukai Y, Kakihana Y, Matsuyama H. Effect of solidification rate of polymer solution on the die-swell during hollow fiber spinning by non-solvent induced phase separation. *J Membr Sci*. 2014;472:194–201.
37. Su Y, Lipscomb G, Balasubramanian H, Lloyd DR. Observations of recirculation in the bore fluid during hollow fiber spinning. *AIChE J*. 2006;52:2072–2078.
38. Li X, Cai T, Chung TS. Anti-fouling behavior of hyperbranched polyglycerol-grafted poly(ether sulfone) hollow fiber membranes for osmotic power generation. *Environ Sci Technol*. 2014;48:9898–9907.
39. Yampolskii Y, Freeman BD. *Membrane Gas Separation*. Singapore: John Wiley & Sons Ltd, 2010.
40. He T, Blume I. A process for drying a wet porous membrane structure. Eur. Patent EP1466659A1, 2004.
41. Brown BM, Ray EL. Method for treating reverse osmosis membranes. U.S. Patent 3773072, 1973.
42. Qin JJ, Li Y, Lee LS, Lee H. Cellulose acetate hollow fiber ultrafiltration membranes made from CA/PVP 360 K/NMP/water. *J Membr Sci*. 2003;218:173–183.
43. Li X, Zhang S, Fu FJ, Chung TS. Deformation and reinforcement of thin-film composite (TFC) polyamide-imide (PAI) membranes for osmotic power generation. *J Membr Sci*. 2013;434:204–217.
44. Youm KH, Kim WS. Prediction of intrinsic pore properties of ultrafiltration membrane by solute rejection curves: effects of operating conditions on pore properties. *J Chem Eng Jpn*. 1991;24:1–7.
45. Hsieh FH, Matsuura T, Sourirajan S. Reverse osmosis separations of polyethylene glycols in dilute aqueous solutions using porous cellulose acetate membranes. *J Appl Polym Sci*. 1979;23:561–573.
46. Singh S, Khulbe K, Matsuura T, Ramamurthy P. Membrane characterization by solute transport and atomic force microscopy. *J Membr Sci*. 1998;142:111–127.
47. Van der Bruggen B, Vandecasteele C. Modelling of the retention of uncharged molecules with nanofiltration. *Water Res*. 2002;36:1360–1368.
48. Wang KY, Yang Q, Chung TS, Rajagopalan R. Enhanced forward osmosis from chemically modified polybenzimidazole (PBI) nanofiltration hollow fiber membranes with a thin wall. *Chem Eng Sci*. 2009;64:1577–1584.
49. Zhang S, Fu FJ, Chung TS. Substrate modifications and alcohol treatment on thin film composite membranes for osmotic power. *Chem Eng Sci*. 2013;87:40–50.
50. Li X, Wang KY, Helmer B, Chung TS. Thin-film composite membranes and formation mechanism of thin-film layers on hydrophilic cellulose acetate propionate substrates for forward osmosis processes. *Ind Eng Chem Res*. 2012;51:10039–10050.

51. Espenan JM, Aptel P. Outer skinned hollow-fibers-spinning and properties. *Membranes and Membrane Processes*. Italy: Springer, 1986:151–161.
52. Widjojo N, Chung TS. Thickness and air gap dependence of macrovoid evolution in phase-inversion asymmetric hollow fiber membranes. *Ind Eng Chem Res*. 2006;45:7618–7626.
53. Peng N, Chung TS, Wang KY. Macrovoid evolution and critical factors to form macrovoid-free hollow fiber membranes. *J Membr Sci*. 2008;318:363–372.
54. Shen X, Zhao Y, Feng X, Zhang Q, Chen L. Temperature-sensitive PVDF hollow fiber membrane fabricated at different air gap lengths. *Polym Eng Sci*. 2013;53:2519–2526.
55. Vogrin N, Stropnik C, Musil V, Brumen M. The wet phase separation: the effect of cast solution thickness on the appearance of macrovoids in the membrane forming ternary cellulose acetate/acetone/water system. *J Membr Sci*. 2002;207:139–141.
56. Li DF, Chung TS, Ren JZ, Wang R. Thickness dependence of macrovoid evolution in wet phase-inversion asymmetric membranes. *Ind Eng Chem Res*. 2004;43:1553–1556.
57. Strathmann H, Kock K, Amar P, Baker RW. The formation mechanism of asymmetric membranes. *Desalination*. 1975;16:179–203.
58. Khayet M. The effects of air gap length on the internal and external morphology of hollow fiber membranes. *Chem Eng Sci*. 2003;58:3091–3104.
59. McCutcheon JR, Elimelech M. Influence of concentrative and dilutive internal concentration polarization on flux behavior in forward osmosis. *J Membr Sci*. 2006;284:237–247.

*Manuscript received May 12, 2015, and revision received July 21, 2015.*